The Astrophysical Journal, 646:1335–1348, 2006 August 1

MAGNETIC STRUCTURES OF SOLAR ACTIVE REGIONS, FULL-HALO CORONAL MASS EJECTIONS, AND GEOMAGNETIC STORMS

Y. Liu,[1] D. F. Webb,[2,3] and X. P. Zhao[1]
Received 2006 February 6; accepted 2006 April 8

ABSTRACT

We have analyzed three active regions to investigate the relationship between magnetic configurations of active regions and geomagnetic storms. Each active region was associated with multiple full-halo coronal mass ejections (CMEs). This study demonstrates that, although full-halo CMEs may originate from the same active region, it is not necessary for them to have similar geoeffectiveness, depending on the magnetic configurations actually involved in the corresponding flare activities. This implies that (1) the flares, CMEs, and geomagnetic storms are closely related magnetically, as already suggested by many others, and (2) the occurrence of solar active region–related geomagnetic storms may be determined by the magnetic fields that are involved in the corresponding solar flares. These associations suggest ways to improve geomagnetic storm prediction.

Subject headings: Sun: activity — Sun: coronal mass ejections (CMEs)

1. INTRODUCTION

On significantly different spatial scales, flares and CMEs are two major manifestations of eruptive release of energy. Flares usually occur in active regions, showing disturbances within localized areas. It is thus considered that flares are related to small-scale magnetic fields. CMEs, on the other hand, are deemed to be large-scale or even global phenomena, related to the large-scale magnetic field. Although there is still uncertainty about the relationship between flares and CMEs, observations give increasing evidence that at least the timing of some CMEs are highly associated with flares (see, e.g., Zhang et al. 2001).

It is generally believed that long intervals of enhanced southward interplanetary magnetic field (IMF) and the high solar wind speed are the primary causes of intense geomagnetic disturbances, and that the solar sources of such geoeffective solar wind structures are usually CMEs (Webb et al. 2001, and references therein).[4] However, not all Earth-directed CMEs can produce geomagnetic storms. Evidence has been presented that the properties of the Earth-directed CMEs, such as the internal structure of the magnetic field, may determine whether or not a geomagnetic storm subsequently occurs (see, e.g., Burton et al. 1975; Cane et al. 2000).

This suggests that the magnetic field serves as a link between flares, CMEs, and geomagnetic storms. As flares usually occur in active regions, it is natural to ask if the configuration of magnetic field of active regions is an essential factor determining whether the related events are geoeffective. In fact, several studies were conducted to establish this link. Pevtsov & Canfield (2001) analyzed geomagnetic events temporally associated with eruptions of active regions with coronal X-ray sigmoids in the period from 1991 to 1998. They found that "there is a clear tendency for sigmoids with leading southward fields to be associated with stronger geomagnetic storms and for those with leading northward fields to be associated with weaker ones." They also found an increase of strong geomagnetic storms after 1996, the solar minimum, which cannot be described reasonably by the scenario that the large-scale dipole field determines geoeffectiveness (see, e.g., Crooker 2000, and references therein). They thus suggested that the magnetic structure of individual active regions plays a role in geomagnetic events. Leamon et al. (2002) extended this work by using a larger sample in the period from 1991 to 2000. They found that the leading fields in magnetic clouds show a weak, solar cycle–based correlation, implying that the toroidal fields of individual active regions are related directly to their heliospheric structure. In a further study, however, they estimated the magnetic twists of the magnetic clouds and their related active regions, and demonstrated that "there is no systematic sign or amplitude relationship between them" (Leamon et al. 2004). The measure of magnetic twist of an active region used there is the multiplication of the average force-free α of the active region by the size of the active region.

Thus, we are still far from establishing a detailed correlation between solar active regions and geomagnetic storms, although interest has been increasing in understanding the role of active regions in the occurrence of geomagnetic storms, and evidence has already been presented to demonstrate a magnetic link. Specifically, it is still unclear whether geomagnetic storms depend on the magnetic configurations of the related active regions. To investigate this question, in this paper, we study the magnetic configuration of the active regions that were associated with multiple full-halo CMEs. The basic hypothesis we are investigating is that if the magnetic configuration of the active regions is a key factor for determining occurrence of geomagnetic storms, the full-halo CMEs originating from the same active region should produce similar degrees of geoeffectiveness. If not, what causes the difference?

This paper is organized as follows. In § 2, we give a list of active regions that are used in this research. This list is based on two existing databases. Each active region was associated with multiple full-halo CMEs, and the CMEs were associated with solar flares. Their geoeffectiveness was determined independently. In § 3, we present the detailed magnetic configurations of the active regions and explore the relationship of those configurations and their geoeffectiveness. We summarize our results in § 4, together with a brief discussion.

2. ACTIVE REGIONS AND RELATED ACTIVITIES

We search for active regions from two databases. One is Table 2 in Zhang et al. (2003). This table contains the geomagnetic

[1] W. W. Hansen Experimental Physics Laboratory, Stanford University, Stanford, CA 94305-4085.
[2] Institute for Scientific Research, Boston College, Chestnut Hill, MA 02467.
[3] Also at: Air Force Research Laboratory, Hanscom Air Force Base, MA 01731.
[4] Very recently, studies showed that some corotating interaction regions (CIRS) can also produce intense storms (Richardson et al. 2006).

TABLE 1
ACTIVE REGIONS WITH MULTIPLE HALO CMES AND THEIR GEOEFFECTIVENESS

Eruption Number (1)	Flare (2)	Date (3)	Time[a] (UT) (4)	Source (5)	Location (deg) (6)	Time (month day, hr) (7)	Storm Dst (nT) (8)
1[b]	M4.2	1997 Nov 3	10:18	AR 8100	S20, W15		None
2[b,c]	X2.1/2B	1997 Nov 4	05:54	AR 8100	S14, W33	Nov 7, 02	−110
3[c]	X9.4/2B	1997 Nov 6	11:22	AR 8100	S18, W63	Nov 7, 02	−54
4[b,c]	C5.2/SF[d]	1998 Nov 4	03:14	AR 8375	N17, E01	Nov 7, 14	−81
5[c]	C5.0/SN	1998 Nov 5	00:20	AR 8375[e]	N19, W11	Nov 8, 01	−149
	C7.1/SF	1998 Nov 5	01:21	AR 8375[e]			
6[b,c]	M8.4/2B	1998 Nov 5	18:31	AR 8375	N22, W18	Nov 8, 06	−142
7[c]	X2.3/3B	2000 Jun 6	15:00[f]	AR 9026	N20, E18	Jun 8, 18	−87
8[c]	X1.2/3B	2000 Jun 7	15:04	AR 9026	N23, E03	Jun 10, 08	−56
9[c]	M5.2/3B	2000 Jun 10	16:37	AR 9026	N22, W38		None

[a] Flare start time from the *Solar Geophysical Data*.
[b] Event identified by Zhang et al. (2003).
[c] Event identified by D. F. Webb (2004, private communication).
[d] D. F. Webb in his table identified this event associated with a C4/SN flare occurred at 03:14 or a C5/SF flare at 03:30, or both. The *SEC Weekly Report* combines the two flares as a C5.2/SF flare lasting from 03:14 to 04:07, although there are two possible peaks in the *Geostationary Operational Environmental Satellite* (*GOES*) X-ray profile. Checking the Hα images shown in Fig. 7 of Zhang & Wang (2001), we can see that these two flares were actually associated with eruption of one filament. The C5/SF flare was associated with the continuous eruption of the low part of the filament. So, as a reasonable approximation for the purpose of this study, we regard these two flares as one in the analysis.
[e] D. F. Webb identified this event as probably associated with multiple flares: a C5/SN flare at 00:20 and another C7/SF flare at 01:20. The *GOES* X-ray profile clearly shows these two flares. Both were reported in the *SEC Weekly Report*. The bright ribbon patterns of these two flares are similar.
[f] The onset of the flare X2.3/3B was 15:00 UT, but it was reported as 12:06 UT in the *SEC Weekly Report*. Actually, that is the onset of an earlier X1.1/2N flare that occurred at the same place of the later ones. The *GOES* X-ray flux profile clearly shows two separate peaks.

storm–related full-halo CMEs from 1996 to 2000. Solar disk source regions of those CMEs were carefully identified using observations such as *Solar and Heliospheric Observatory* (*SOHO*) Extreme ultraviolet Imaging Telescope (EIT) for solar transient determination. The other is from D. F. Webb (2004, private communication), who studied 134 full-halo CMEs observed by Large Angle and Spectrometric Coronagraph Experiment (LASCO) from 1996 to 2000 (see also Zhao & Webb 2003). A geomagnetic storm in that study was defined by the peak Dst < -50 nT. Solar disk regions for those CMEs were determined using observations such as Hα, *Yohkoh* X-ray, and EIT images.

The criteria for selection of the events for this paper are that (1) the active regions were associated with multiple full-halo CMEs, (2) each CME was associated with one solar flare (but multiple flares for event 5; see Table 1 note for more details), and (3) its geoeffectiveness was determined. Three active regions were chosen for this study (see Table 1). Column (1) of this table is the identification number of the eruption. Footnotes b and c denote the original source of the data. Columns (2)–(4) are flare size, date, and time, respectively. Here, the flare time represents the flare start time from the *SEC Weekly Report: The Preliminary Report and Forecast of Solar Geophysical Data*.[5] Columns (5) and (6) are the solar disk active region numbers and their disk coordinates, respectively. The date and time, and peak Dst of the related geomagnetic storms are presented in columns (7) and (8), respectively.

3. RESULTS

Each flare location was aligned to the relative *SOHO* MDI magnetograms (Scherrer et al. 1995) in order to explore the magnetic configuration associated with the flare. The alignment for the data taken by *SOHO* and *Yohkoh* was done using the IDL map software in the Solar SoftWare (SSW) written by D. Zarro.

[5] Available at http://www.sec.noaa.gov/weekly.

3.1. *Active Region AR 8100*

Active region AR 8100 produced three flares associated with full-halo CMEs: M4.2 occurred at 10:18 UT of 1997 November 3, X2.1/2B at 05:54 UT of November 4, and X9.4/2B flare at 11:22 UT of November 6 (see Table 1). We denoted these flares as "F1," "F2," and "F3." Figure 1 shows an EIT image taken at 10:21 UT, overplotted in contours by an MDI magnetogram

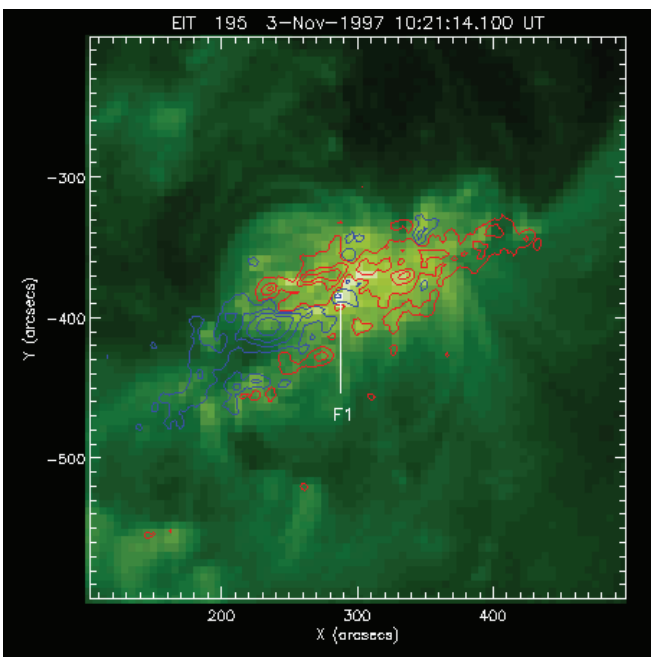

FIG. 1.—Alignment of *SOHO* EIT and MDI data. An EIT image at 195 Å wavelength, taken at 10:21 UT on 1997 November 3, is overplotted in contours by a MDI magnetogram taken at 11:05 UT of 1997 November 3. The red (*blue*) lines represent positive (*negative*) magnetic field. Solar rotation was corrected for. The bright pattern, marked by F1, was the location of the 10:18 UT M4.2 flare.

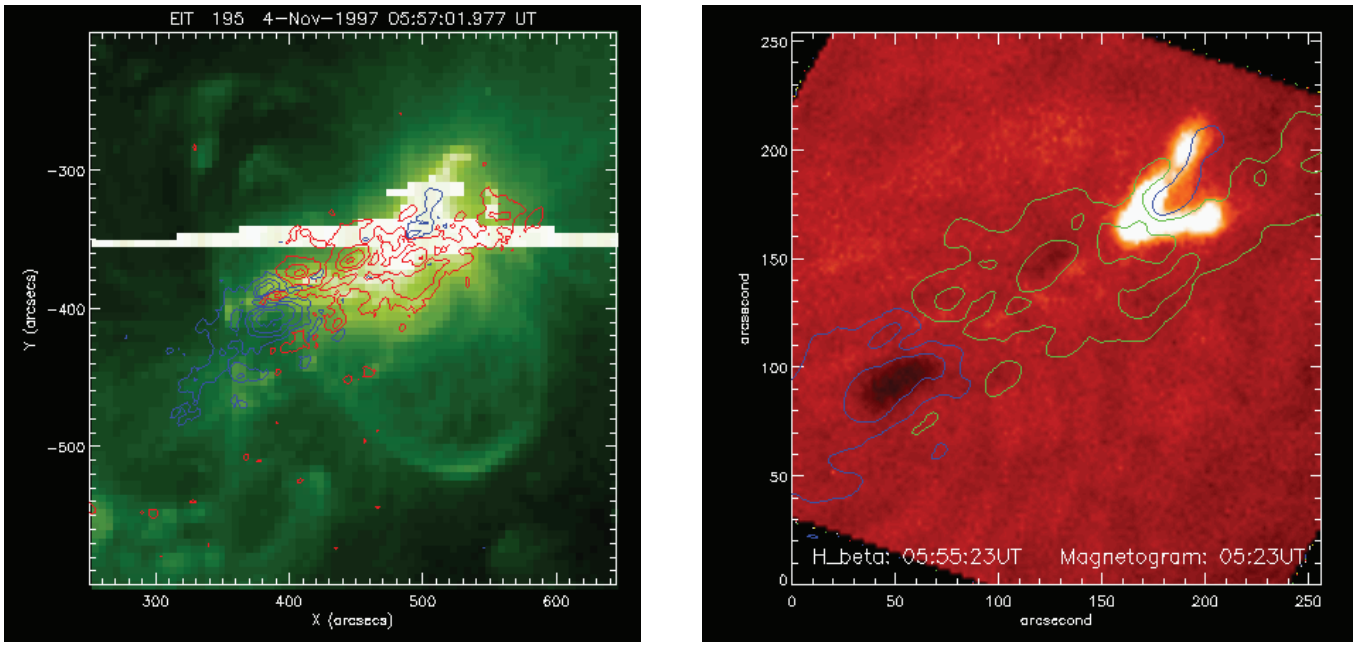

FIG. 2.—*Left:* EIT image overplotted by a MDI magnetogram, as Fig. 1. The EIT and MDI data were taken, respectively, at 05:57 and 06:27 UT of 1997 November 4. The EIT image was saturated due to the 05:54 UT X2.1/2B flare (F2). *Right:* Hβ image overplotted by a line-of-sight magnetogram. The data were taken at 05:55 UT (Hβ image) and at 05:23 UT (magnetogram) at HSOS. The bright pattern in the Hβ was the flare F2.

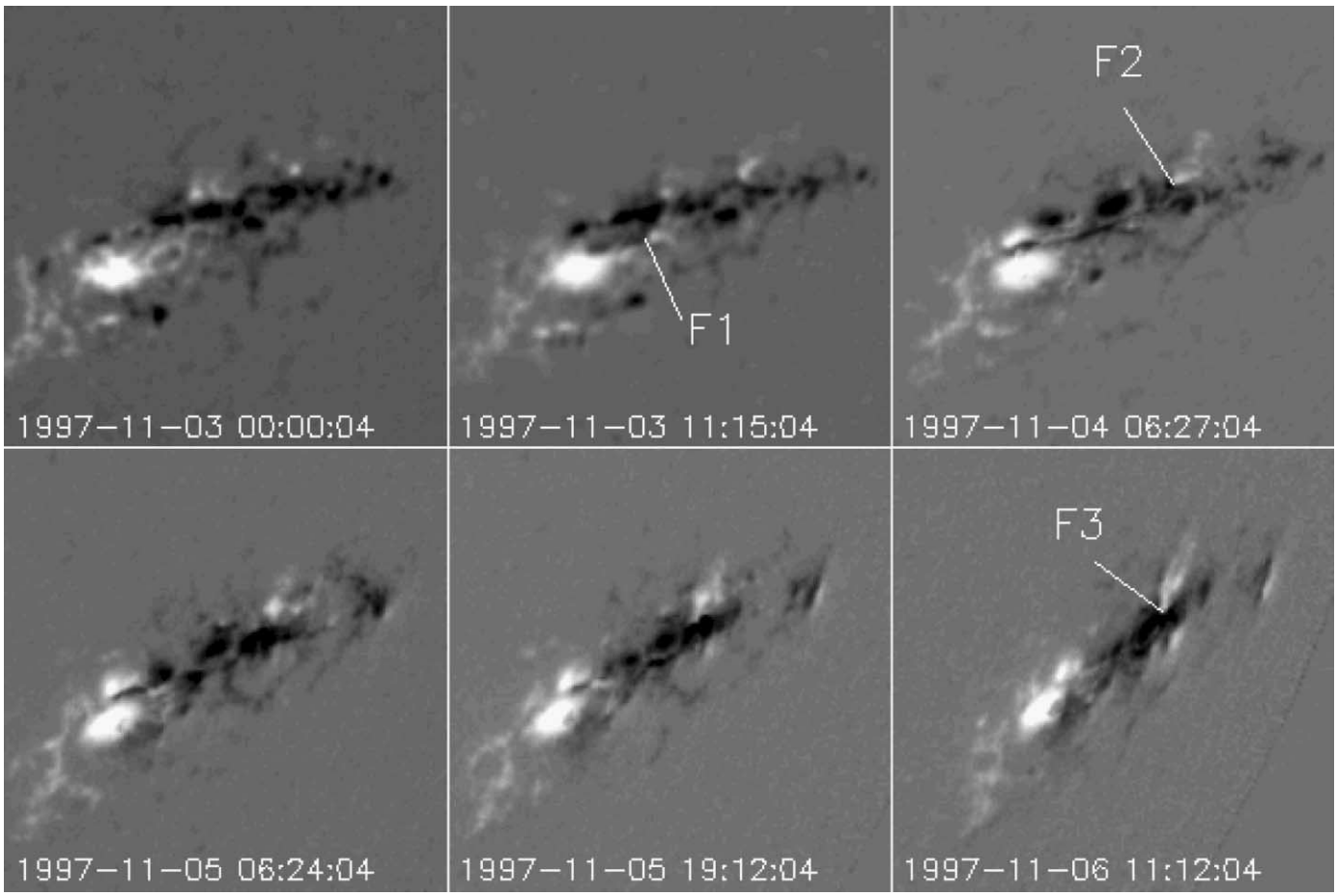

FIG. 3.—Evolution of magnetic field of the active region AR 8100 from 1997 November 3–6. The marks F1, F2, and F3 denote the locations of the M4.2, X2.1/2B, and X9.4/2B flares, respectively. The field of view is $300'' \times 300''$. Time goes from left to right and top to bottom.

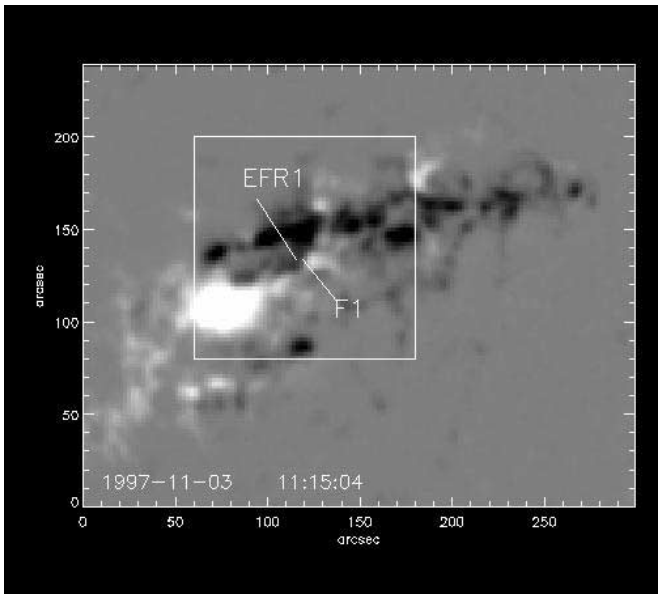

FIG. 4.—MDI magnetogram taken at 11:05 UT of 1997 November 3. White (*black*) represents positive (*negative*) polarity. Emerging magnetic flux (marked as EFR1) was found to be associated spatially with the flare F1, as seen in Fig. 1.

taken at 11:05 UT. The initial brightening of flare F1 is marked by F1.

We displayed in the left panel of Figure 2 an EIT image taken at 05:57 UT of November 4, overplotted by the 06:27 MDI magnetogram. As the EIT image was saturated due to flare F2, an Hβ image, taken at 05:55 UT at Huairou Solar Observing Station (HSOS), is presented in the right panel. Overplotted in the right panel is a magnetogram taken at 05:23 UT at HSOS. The location of flare F2 was then determined. The location of flare F3 was determined by aligning the *Yohkoh* soft X-ray images with an MDI magnetogram.

We showed in Figure 3 the evolution of the magnetic field of AR 8100 from November 3–6. The locations of flares F1–F3 are also marked in the figure. It is seen that F2 and F3 occurred at the same location, while the earlier flare F1 occurred east of this.

Magnetic field observation seems to suggest that the magnetic field involved in the F2 and F3 flares is different from that in the F1 flare. Figure 4 shows the magnetic configuration for the F1 flare. It appears to be associated with an elongated negative magnetic feature, marked as "EFR1." This feature was an emerging flux region. It appeared first at the middle of the active region in the MDI 1997 November 3 08:03 magnetogram (see Fig. 5) and elongated afterward. Flares F2 and F3, on the other hand, occurred at the area F2 (see Fig. 6). They appeared to be related to a positive

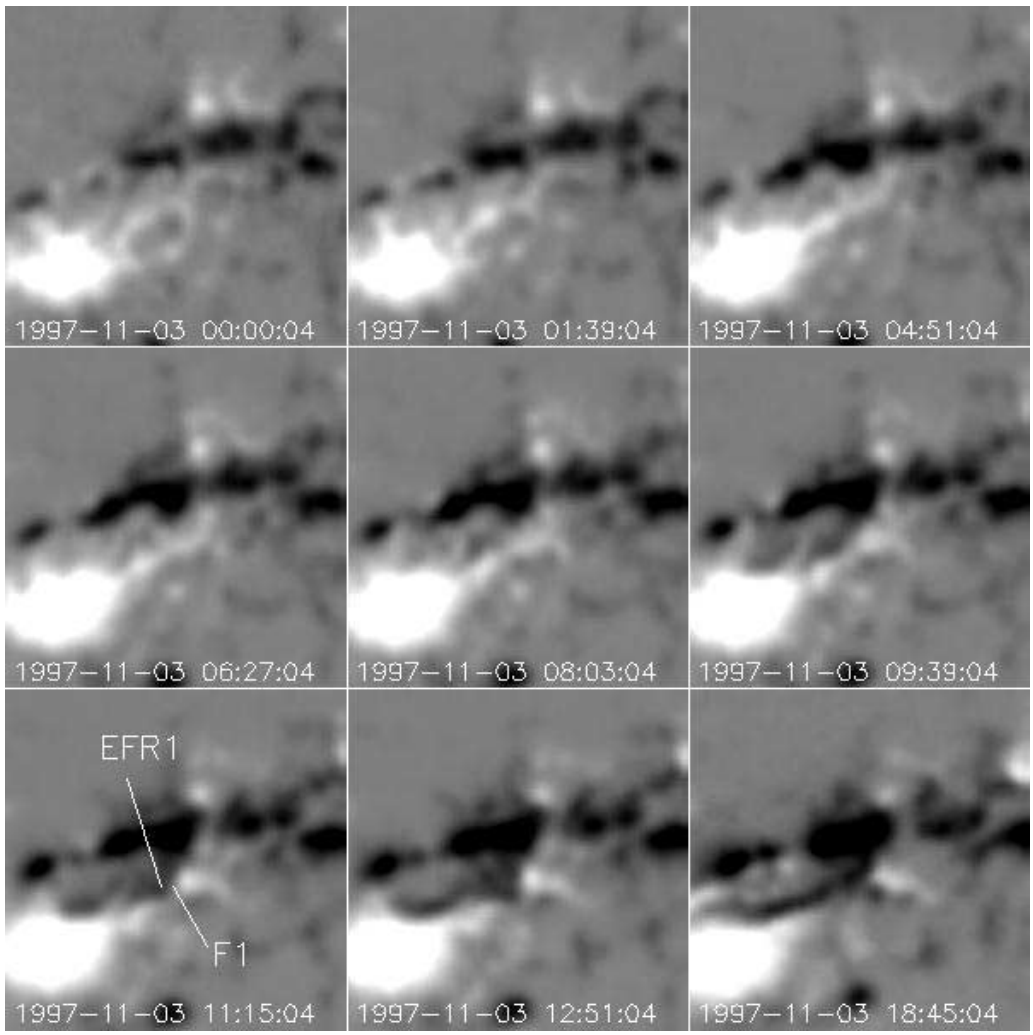

FIG. 5.—Series of enlarged MDI magnetograms shows the evolution of magnetic field in the square area in Fig. 4. The magnetic flux, marked by EFR1 in the bottom left panel, was seen to emerge quickly. This emerging flux region appears to be associated with the flare F1. The field of view is $120'' \times 120''$. Time goes from left to right and top to bottom.

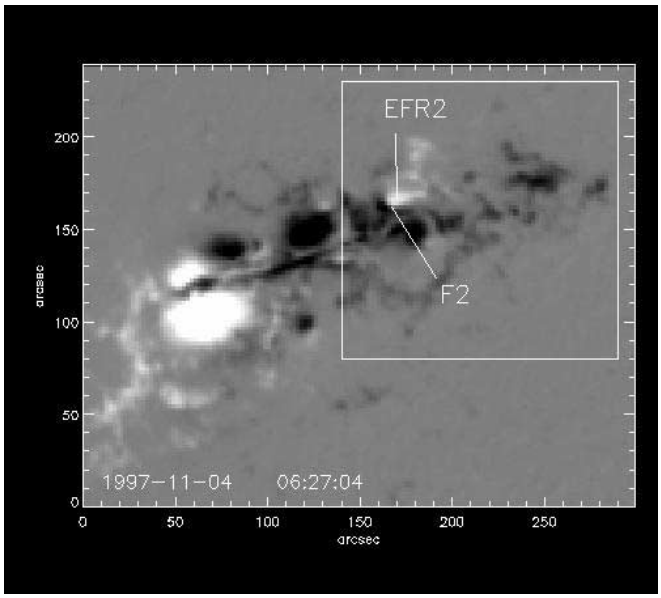

FIG. 6.—MDI magnetogram taken at 06:27 of 1997 November 4. The F2 flare occurred along a magnetic neutral line between the positive field patch (marked as EFR2) and the negative field.

magnetic patch, marked as "EFR2" in Figure 6. This patch, first seen in the MDI 1997 November 2 22:24 magnetogram (see Fig. 7), was likely to be another emerging flux region. It continued emerging and developing in the following days (see Fig. 8).

The magnetic structure of this active region may be represented by an extrapolated nonlinear force-free magnetic field. The *Yohkoh* soft X-ray bright patterns above this region and the change of the patterns from November 3 to 4 were reproduced successfully by a nonlinear force-free field calculation (Liu et al. 2002). We plotted in Figure 9 the field lines extrapolated from a photospheric vector magnetogram taken at 00:56 UT of November 4 at HSOS using a boundary integral equation representation proposed by Yan & Sakurai (2000). From these field lines, we selected those that match well with the *Yohkoh* soft X-ray bright loops/patterns and plotted them in Figure 10. Basically, we see two bipolar magnetic configurations in this active region, shown in white and black lines. Both bipolar fields obey the Hale-Nicholson polarity law (Hale & Nicholson 1938), further verifying such configurations. The small one was clearly related to the emerging flux region EFR2. Flares F2 and F3 occurred at the interface of the two bipolar magnetic fields. Flare F1, on the other hand, occurred beneath the large bipolar field, far away from this interface.

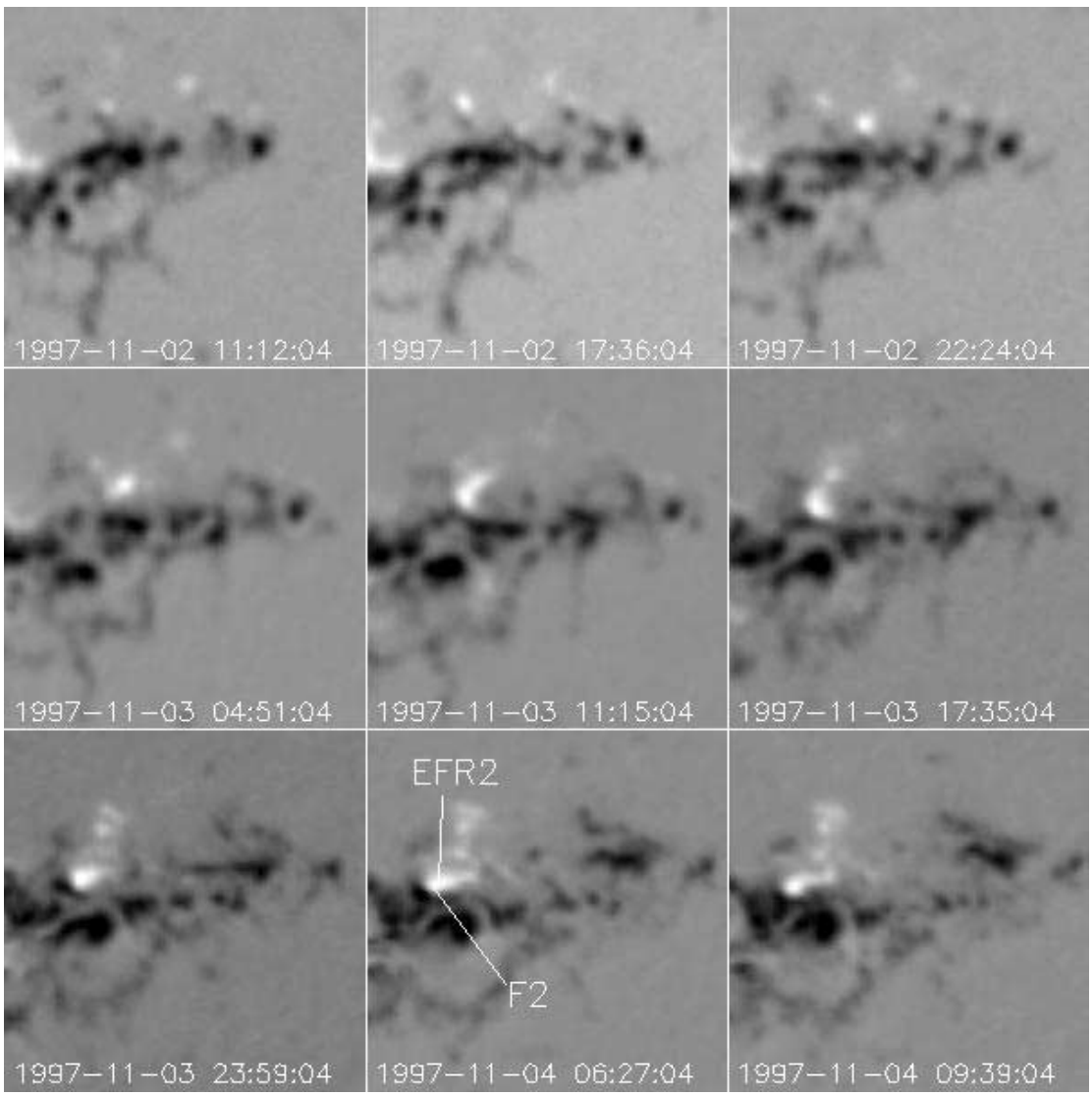

FIG. 7.—Evolution of magnetic field in the square area shown in Fig. 6. It was seen that the emerging magnetic fluxes, denoted by EFR2 and appearing in the November 2 22:24 magnetogram (*top right*), increased dramatically afterward. The field of view is $150'' \times 150''$. Time goes from left to right and top to bottom.

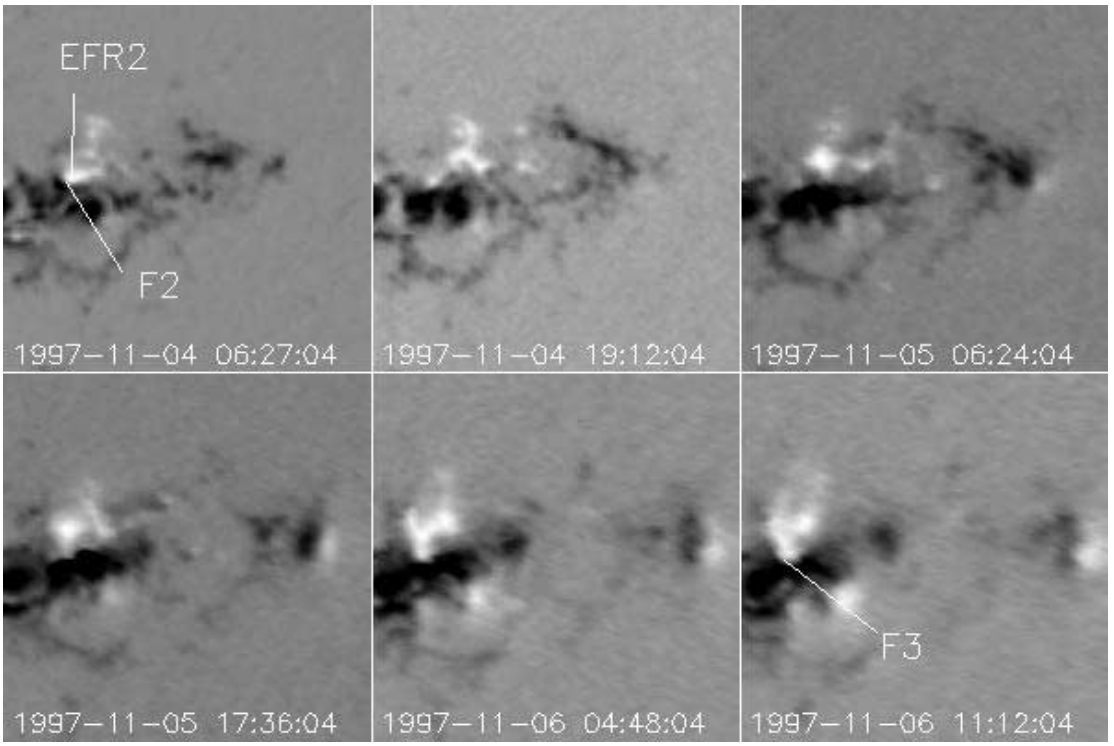

FIG. 8.—Evolution of magnetic field of emerging flux region EFR2 from November 4–6. Flare F2 occurred at the magnetic neutral line between this emerging flux region and an adjacent negative patch. This emerging flux region was also associated spatially with flare F3. A geometric projection effect was corrected for in these magnetograms. The field of view is $200'' \times 200''$. Time goes from left to right and top to bottom.

The small bipolar field configuration was also verified by the vector magnetic field observation. The left panel of Figure 11 shows the vector magnetic field of this active region on the photosphere taken at 05:23 UT of November 4. In the right panel is an enlarged figure displaying the magnetic field of EFR2. This figure demonstrates an evident connectivity from the positive patch of EFR2 (marked by "A") to the negative magnetic field to its right (marked by "B"). This connectivity is consistent with the small bipolar field configuration.

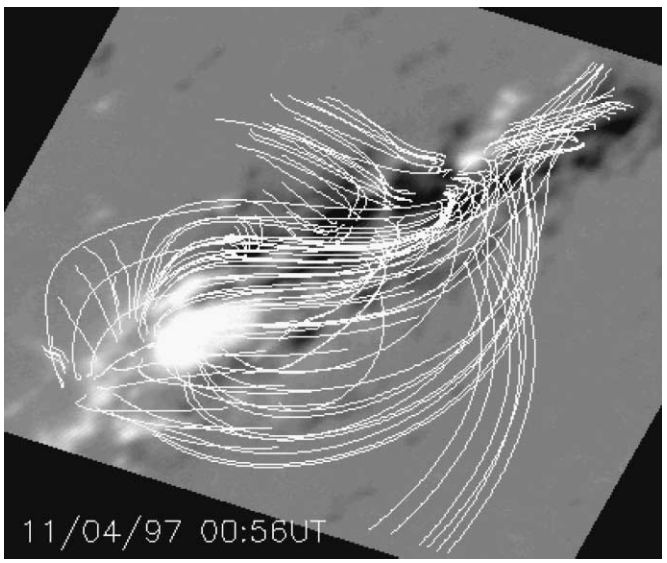

FIG. 9.—Magnetic field lines (*white lines*) computed from a photospheric vector magnetogram under the nonlinear force-free-field assumption. The vector data were taken at 00:56 UT of 1997 November 4 at HSOS. The image shows the line-of-sight component of the magnetic field.

In order to show the large-scale magnetic field involved in those events, we presented in Figures 12–14 the remapped MDI magnetograms in the top panels and the remapped EIT running difference images in the bottom panels. We remapped the images onto the heliospheric coordinates to avoid projection effects because those events occurred 3 days apart, and events F2 and F3 were far away from the disk center. The EIT dimming was clearly seen in those events. Although the level of darkness was probably caused by the magnitudes of the related flares, the dimming areas in all three events connected AR 8100 on the southern hemisphere and AR 8102 on the northern hemisphere, suggesting that the magnetic field connecting the two regions was also involved in the events. In fact, such a transequatorial magnetic system has already been identified from *Yohkoh* soft X-ray images and a potential field modeling (Delannee & Aulanier 1999).

From the above analysis we can see that, although full-halo CMEs associated with flares F1, F2, and F3 were related to the same active region and the large-scale magnetic field involved in these events was similar, their geoeffectiveness was different (see Table 1). Only flares F2 and F3, which occurred at the same location, were found to be associated with geomagnetic storms. This seems to suggest that the magnetic fields that were actually involved in the related flares play a role in determining the occurrence of geomagnetic storms.

3.2. *Active Region AR 8375*

Active region AR 8375 produced three (or four) flares that were associated with full-halo CMEs: C5.2/SF at 03:14 UT of 1998 November 4 (see footnote d of Table 1 for more detail), C7.1/SF at 01:21 UT (and/or C5/SN flare at 00:20 UT) of 1998 November 5, and M8.4/2B at 19:31 UT of 1998 November 5. As the November 5 C5/SN flare is very similar with the C7.1/SF

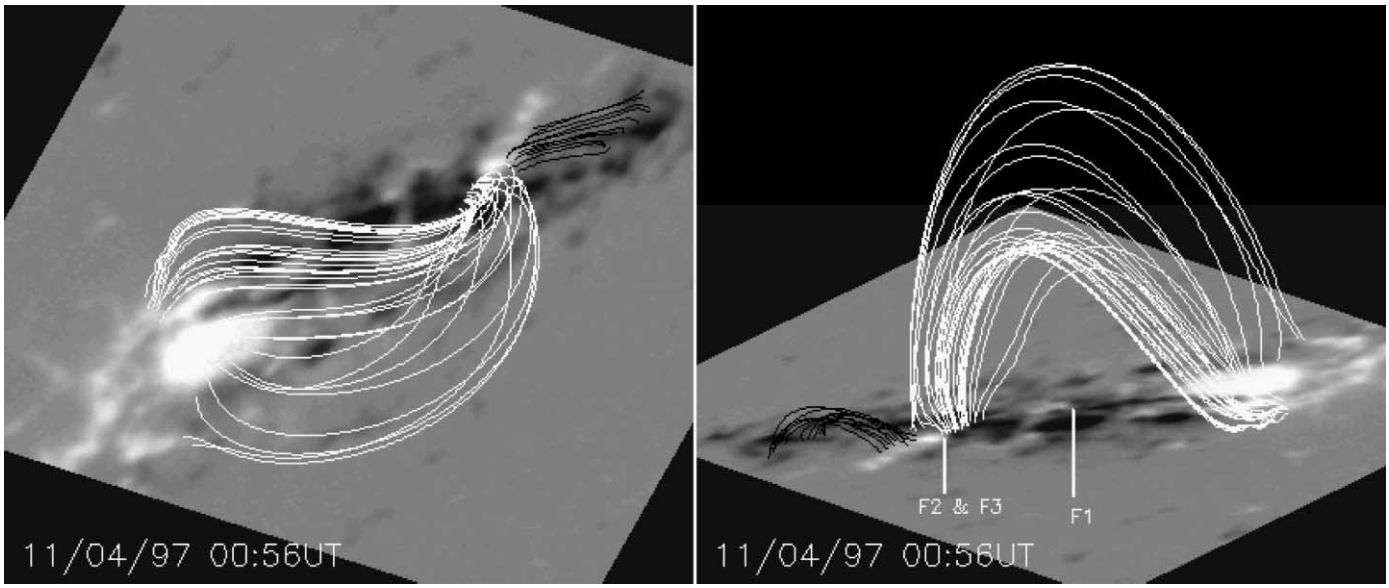

FIG. 10.—Selected field lines viewed from different angles showing the magnetic configuration in this active region. Apparently there are at least two well-defined bipolar magnetic configurations, as demonstrated in white and black field lines. The F2 and F3 flares occurred at the interface of the two bipolar fields.

flare in term of flare locations and their bright patterns,[6] we only use the C7.1/SF flare for event 5. We denoted these flares as "F4," "F5," and "F6," respectively. The same alignment between the EIT images and MDI magnetograms was performed, as described in the beginning of § 3, to determine the locations of these flares. The magnetic configuration of this active region looks fairly simple: a dominant positive magnetic patch surrounded by several small parasitic negative magnetic features (see Fig. 15). The initial brightenings of the flares are found to be associated with three parasitic features, denoted by F4, F5, and F6 in Figure 15. The locations of these features were quite close to each other. All three flares were associated with eruptions of filaments. Presented in Figure 16 are Hα images at the line center before (*left*) and during the flares (*right*).[7] We can clearly see that flares F4, F5, and F6 were associated with eruptions of filament L1 (*top*), filament L2 (*middle*), and filament L3 (*bottom*), respectively. In fact, flares F4 and F6 have been analyzed by Zhang & Wang (2001) and Wang et al. (2000). The eruptions of the filaments (filaments L1 and L3) shown in the Hα images in those papers appeared to be the so-called eruption of a filament layer (Tang 1986); i.e., only an

[6] These two flares were observed in Hα wavelength at Hida Observatory. (Data are available at http://www.kwasan.kyoto-u.ac.jp/observation/event/fmt/lists/FMT-B-Nov98.html.) The first available Hα image, taken at 00:16, only shows two bright ribbons, suggesting that the flare already occurred. Thus, we are not able to identify whether this flare was associated with an eruption of a filament or not, but the pattern of the ribbons seems to imply a filament eruption. Later, a filament formed along the filament channel of the presumably previous erupted filament (see the 00:51 image). Part of this filament disappeared in the 01:20 Hα image, leading to the C5/SN flare. The bright pattern of this flare is similar to that of the 00:16 flare.

[7] Kyoto data are available at http://www.kwasan.kyoto-u.ac.jp/observation/event/fmt/index_en.html.

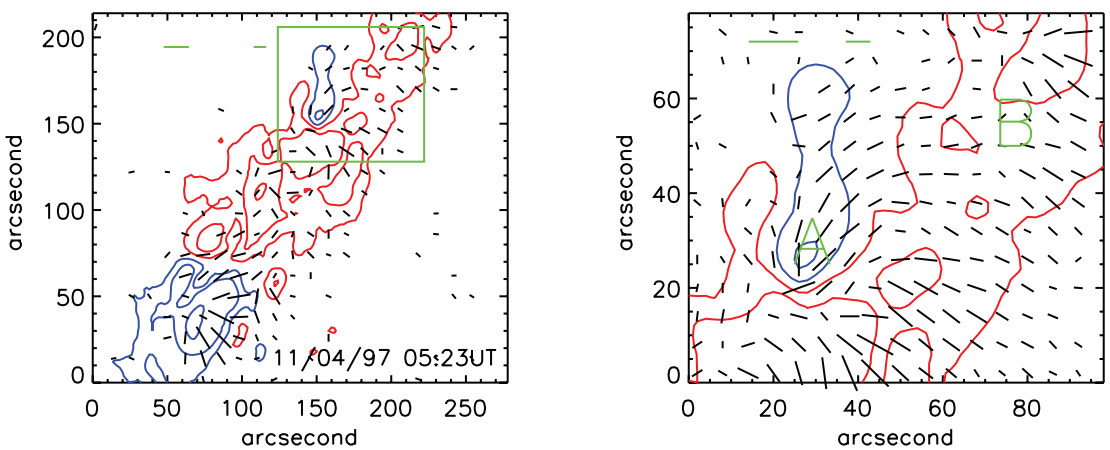

FIG. 11.—*Left:* Photospheric vector magnetic field of the active region AR 8100 taken at 05:23 UT of 1997 November 4 at HSOS. The contours represent the line-of-sight magnetic field with positive polarity in blue and negative polarity in red. The levels of the contours are 40, 120, 360, and 1280 G. The black bars represent the transverse magnetic field, and the right and left green bars at the top denote 1000 and 2000 G, respectively. *Right:* Enlarged vector magnetic field. The field of view, shown as a square in the left panel, covers the emerging flux region EFR2, as described in Fig. 6. The transverse magnetic field shows a tendency for the field to connect with the emerging flux patches A and B.

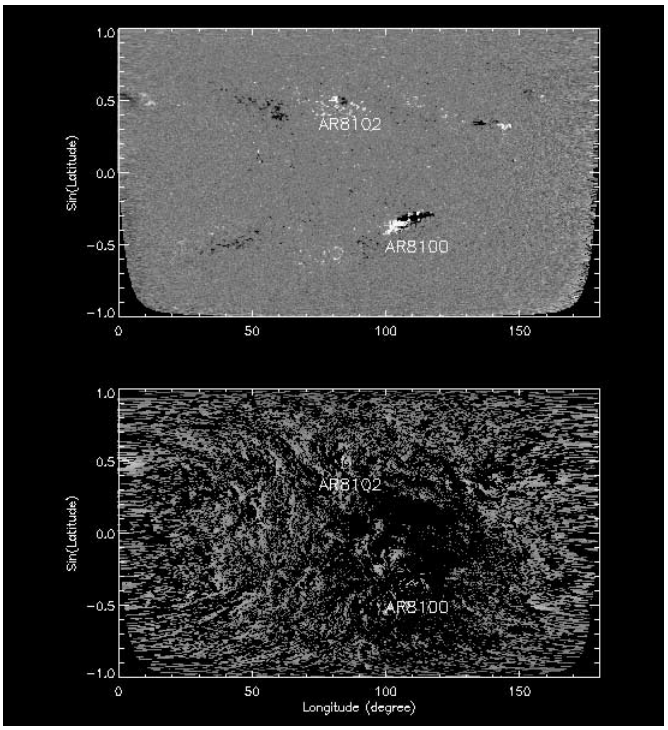

FIG. 12.—Remapped MDI magnetogram (*top*) and EIT running difference image (*bottom*) in heliospheric coordinates. The MDI magnetogram was taken at 11:15 UT of 1997 November 3, while the EIT running difference image was derived from two EIT images taken at 10:33 and 10:50 UT of 1997 November 3.

upper layer peels off, and a low-lying remnant remains in the chromosphere. The eruption of filament L2 (associated with the C7.1/SF flare) also displayed the same kind of eruption as shown in the Hα data taken by Hida Observatory. From their shapes and locations, it is likely that these three filaments belong to the same

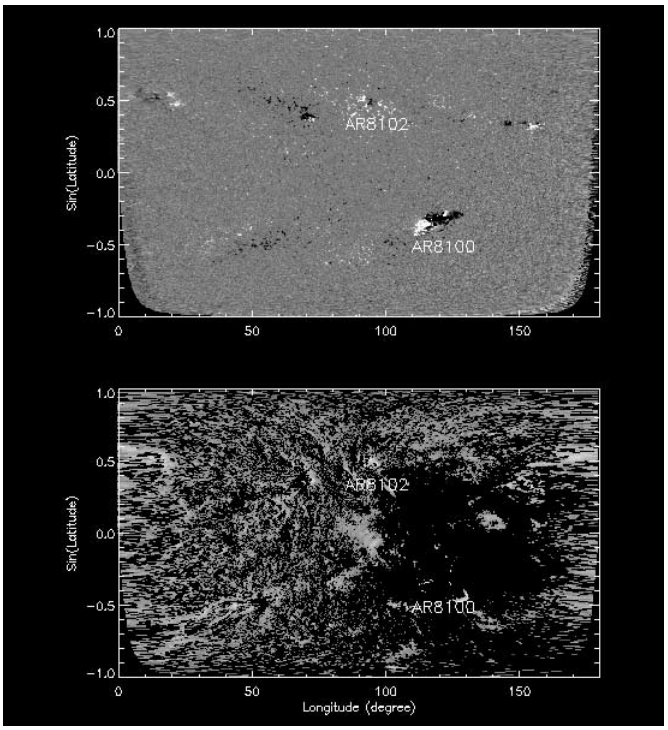

FIG. 13.—Same ass Fig. 12, but for the MDI magnetogram taken at 06:27 UT and the EIT images taken at 05:58 and 06:32 UT of 1997 November 4.

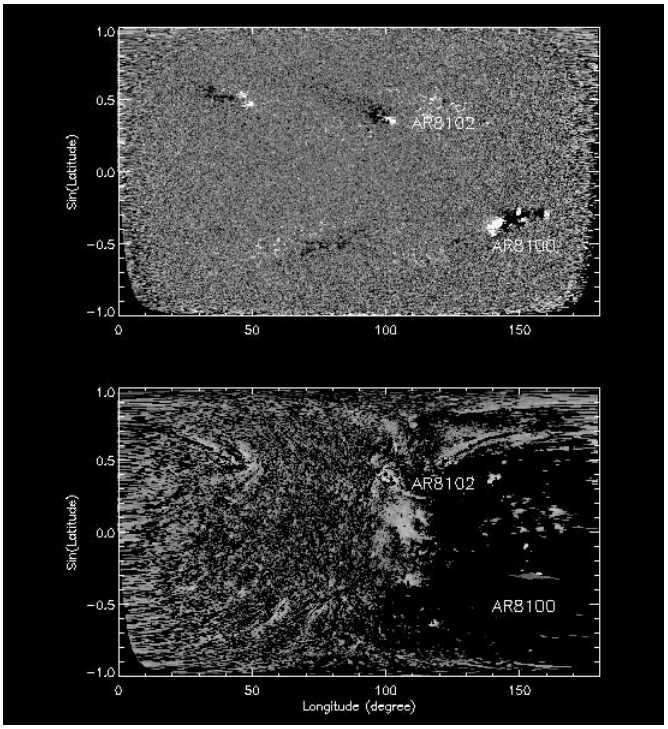

FIG. 14.—Same as Fig. 12, but for the MDI magnetogram taken at 12:48 UT and the EIT images taken at 12:01 and 12:15 UT of 1997 November 6.

"parent filament" (Tang 1986), although observations are not able to provide solid evidence to verify this due to a data gap. It is reasonable to believe that these filaments had very similar structures. Thus, we can expect that the magnetic field involved in those flares had very similar configurations.

The large-scale magnetic field involved in these events was also similar. As with AR 8100, we show in Figures 17–19 the remapped MDI magnetograms and the remapped EIT running difference images. Although very faint, we can still see that, for the three events, the EIT dimming areas connected AR 8375 in the northern hemisphere and AR 8373 in the southern hemisphere, implying a transequatorial magnetic system involved in all three events. Such a connectivity was verified by the *Yohkoh* soft X-ray observation (see Fig. 20).

We have demonstrated here that the magnetic field in the three flares had similar configuration and that the large-scale field involved in these events was also very similar. All three of these full-halo CMEs were associated with large geomagnetic storms (see Table 1).

3.3. *Active Region AR 9026*

The active region AR 9026 also produced three flares that were associated with full-halo CMEs. We denoted these flares as "F7," "F8," and "F9" for the X2.3/3B flare at 15:00 UT of 2000 June 6 (see footnote f of Table 1 for more detail), X1.2/3B flare at 15:04 UT of 2000 June 7, and X5.2/3B flare at 16:37 UT of 2000 June 10, respectively. As before, we determined the locations of the flares by aligning the EIT images with the related MDI magnetograms. A series of magnetograms in Figure 21 was taken from 2000 June 6 to 10, showing the evolution of the magnetic field in this region. The locations of the flares were marked by F7, F8, and F9 on the related magnetograms.

Significant changes in magnetic field can be seen in this period. For example, at the center of the images were two magnetic patches with opposite polarities that decayed markedly from June 6 to 9 and were barely visible on June 10. It is clear that

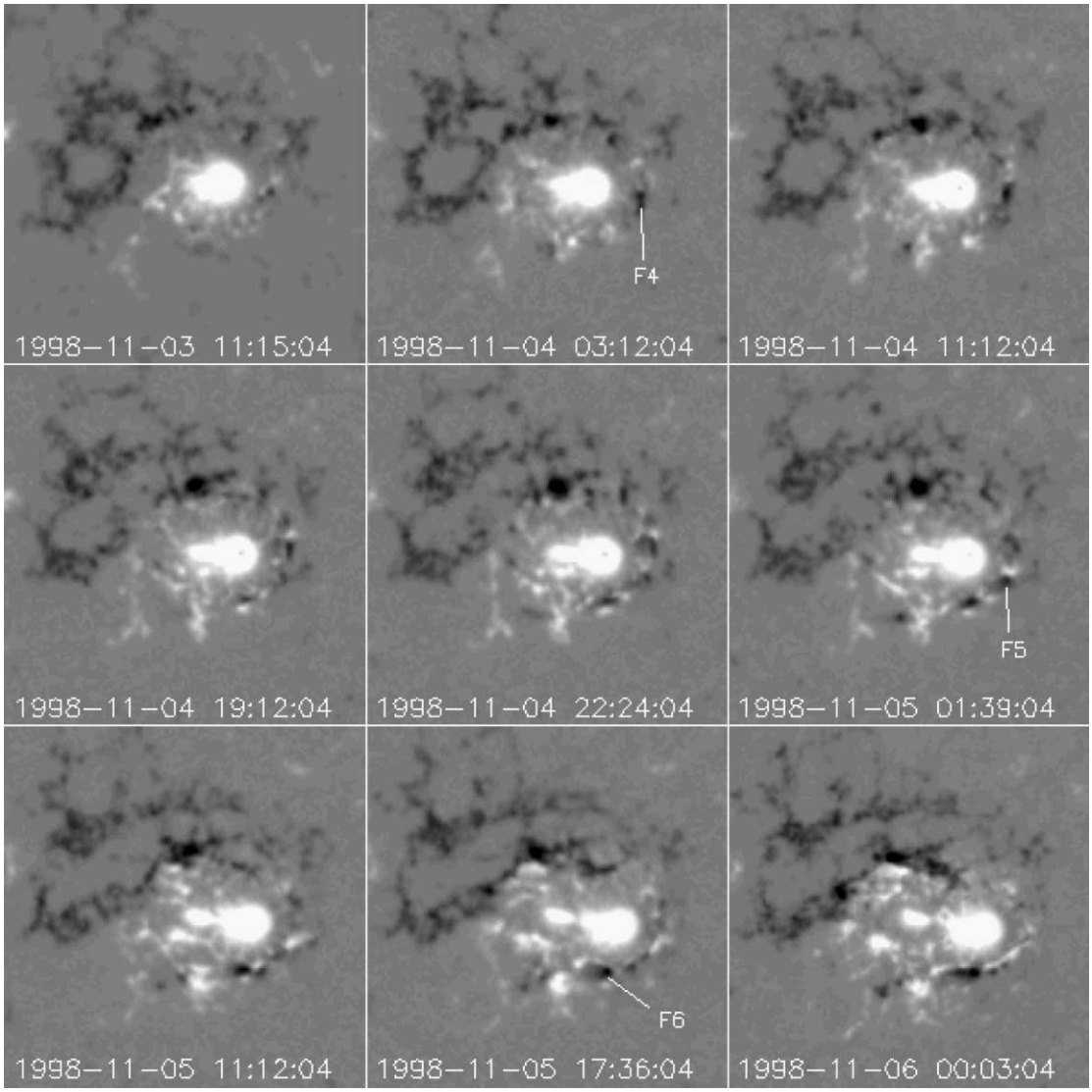

FIG. 15.— Evolution of magnetic field of the active region AR 8375 from November 3–6. The initial brightenings of the three flares are marked by F4, F5, and F6, respectively. It is seen that these locations are very close, and each one was associated spatially with a parasitic magnetic feature surrounding the dominant magnetic patch at the center. The field of view is $240'' \times 240''$. Time goes from left to right and top to bottom.

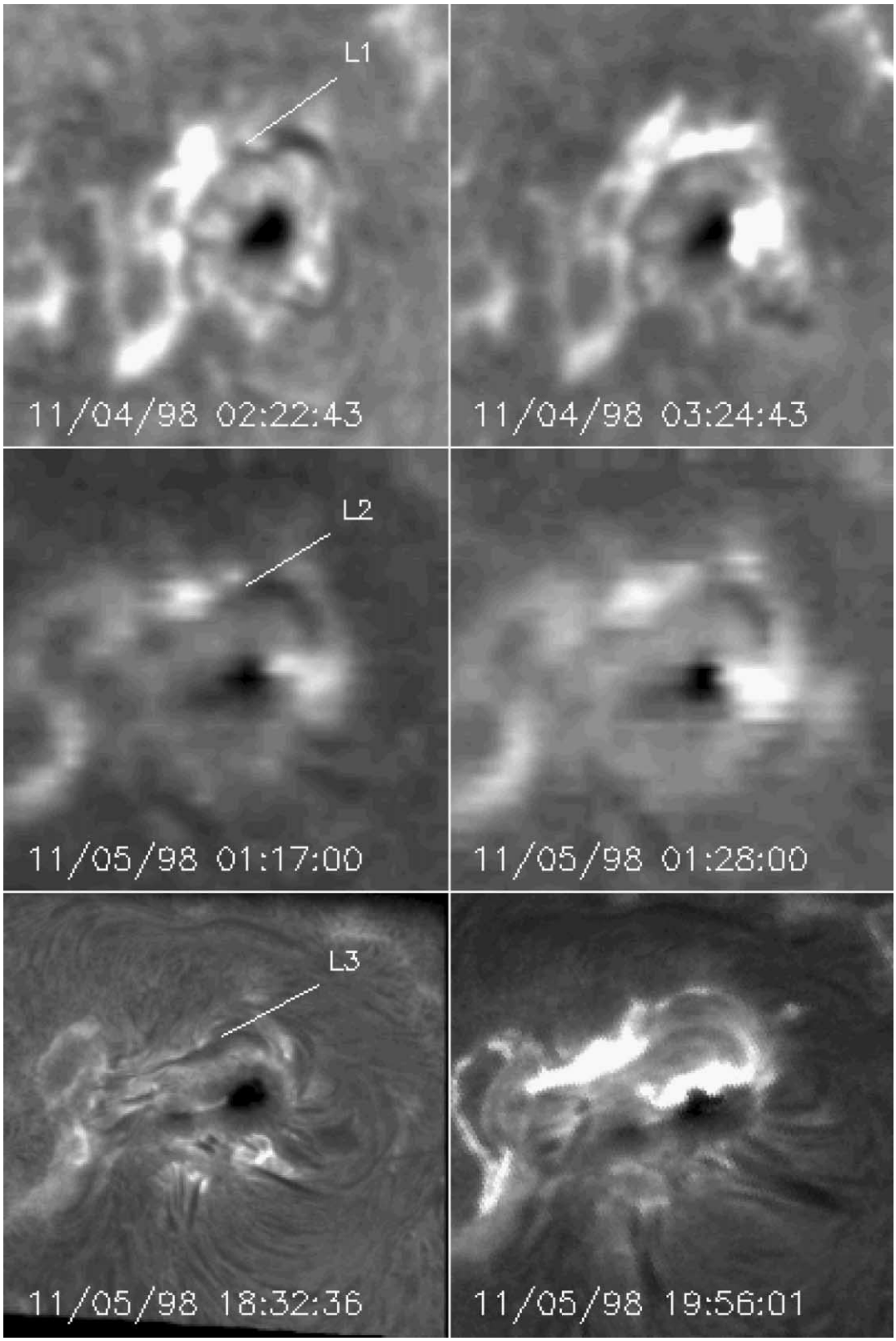

FIG. 16.—Hα line center images taken before the flares (*left*) and during the flares (*right*). The images in the top panels, taken at HSOS of Beijing Astronomical Observatory, show flare F4 and an erupted filament, marked by L1. The images in the middle panels, taken at Kwasan and Hida Observatory of Kyoto University, show flare F5 and filament L2. The images in the bottom panels, taken at Big Bear Solar Observatory (BBSO), show flare F6 and filament L3. The field of view is roughly $200'' \times 200''$.

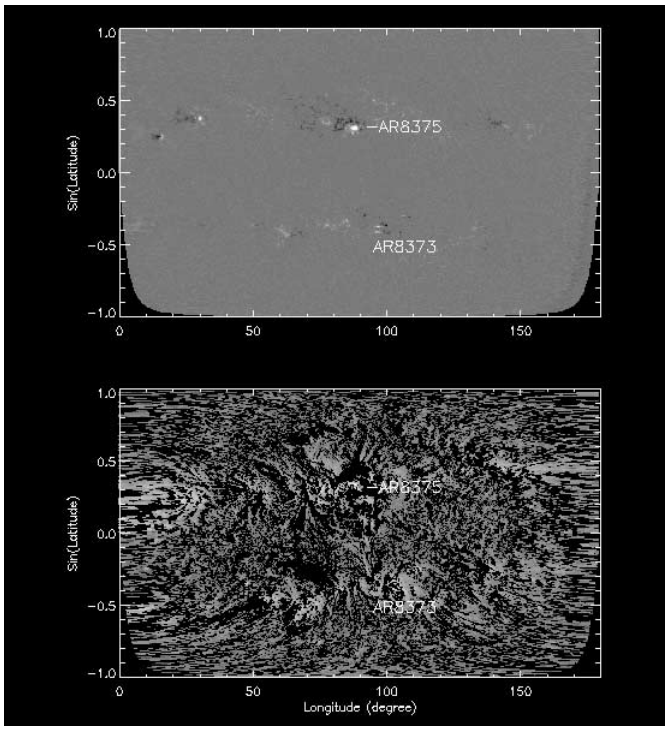

FIG. 17.—Same as Fig. 12, but for the MDI magnetogram taken at 03:12 UT and the EIT images taken at 03:24 and 03:48 UT of 1998 November 4.

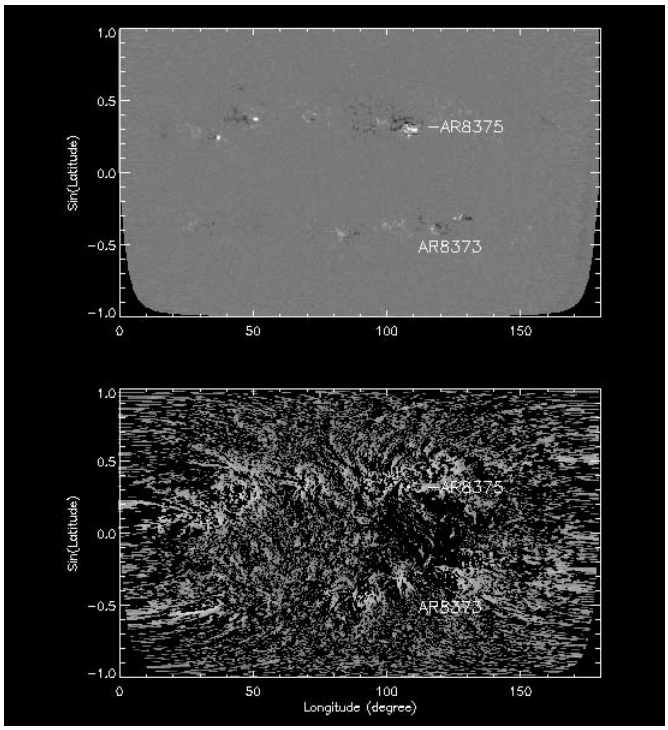

FIG. 19.—Same as Fig. 12, but for the MDI magnetogram taken at 19:12 UT and the EIT images taken at 18:16 and 18:38 UT of 1998 November 5.

flares F7 and F8 occurred at the same region along the neutral line of these two magnetic patches. Although the third flare, F9, occurred geometrically close to this place, the basic configuration of magnetic field in the place had changed; the magnetic patches had disappeared completely in the MDI 2000 June 10 16:00 magnetogram before flare F9 had occurred. The EIT dimming for these events exhibited similar patterns (see Figs. 22–24), implying that the large-scale magnetic field involved in the events had a similar configuration.

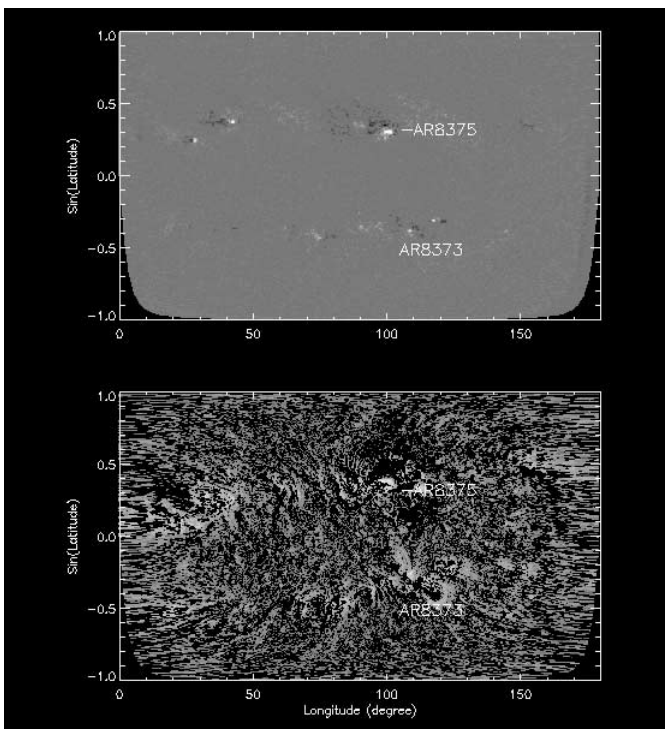

FIG. 18.—Same as Fig. 12, but for the MDI magnetogram taken at 01:39 UT and the EIT images taken at 01:04 and 01:20 UT of 1998 November 5.

It is interesting to note that, although the three flares occurred in the same places and were associated with full-halo CMEs, and the large-scale magnetic field involved in the events was similar, only two flares, F7 and F8, were found to be related to geomagnetic storms. They occurred at the neutral line of the major magnetic patches with opposite signs. These patches had disappeared before the third flare F9 occurred. F9 was not related to any geomagnetic storms.

4. CONCLUSIONS AND DISCUSSIONS

We have analyzed three active regions to explore the relationship between the magnetic structure of active regions and geomagnetic storms. Each active region was associated with multiple full-halo CMEs. The study shows that it is not necessary for the full-halo CMEs to have similar geoeffectiveness, although they originate from the same active region. Further analysis reveals that, although the large-scale magnetic field involved in the CMEs appears to be similar, locations of the associated flares and therefore the magnetic configurations could be totally different. The latter seems to lead to different degrees of geoeffectiveness. More specifically, it is shown that, when the associated flares occurred in the places where the configurations of magnetic fields were identical or similar, the halo CMEs did have similar geomagnetic effects. This implies that the flares, CMEs, and geomagnetic storms are closely related magnetically, as suggested by others (see, e.g., Webb et al. 2000; Zhao & Webb 2003, and references therein). This research also implies that the occurrence of solar active region–related geomagnetic storms may be determined by the magnetic field that is actually involved in the corresponding solar flares. These associations suggest ways to improve geomagnetic storm prediction.

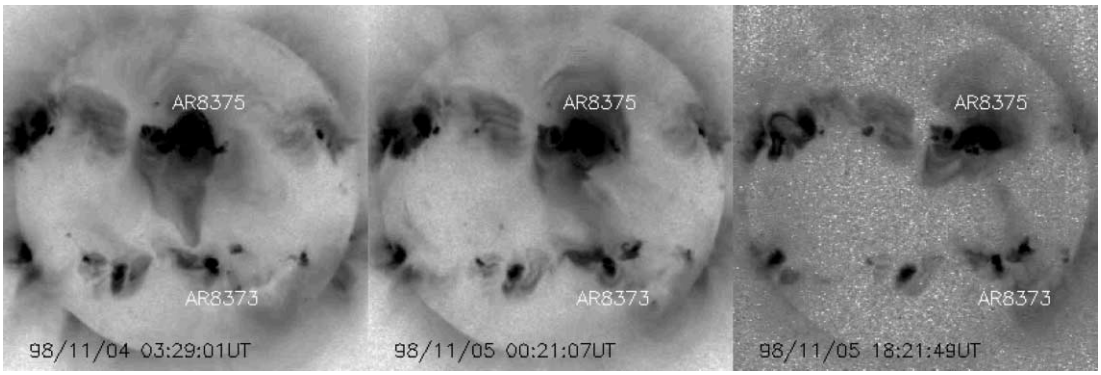

FIG. 20.— Full-disk, soft X-ray images taken by *Yohkoh* SXT at 03:29:01 of 1998 November 4, 00:21:07 of 1998 November 5, and 18:21:49 of 1998 November 5. A transequatorial loop/pattern connecting active regions AR 8375 and AR 8373 can be seen in each image.

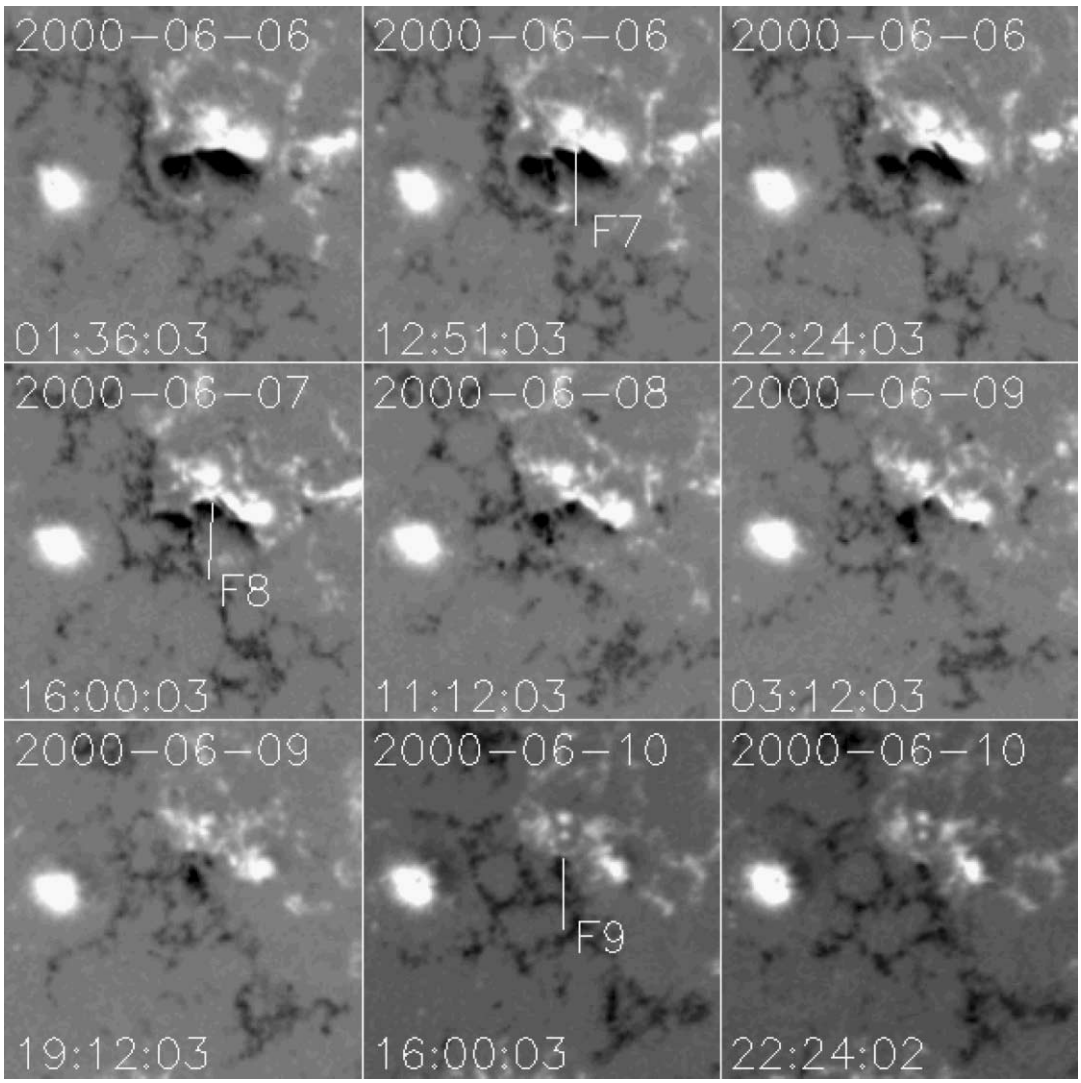

FIG. 21.— Evolution of magnetic field of the active region AR 9026 from 2000 June 6 to 10. The flares are denoted by F7, F8, and F9. While the locations of the flares seem to be very close to each other, the magnetic field involved in the flares F7 and F8 was significantly different from that in flare F9: The magnetic field associated with the flares F7 and F8 had completely disappeared by the time the flare F9 occurred. The field of view is $240'' \times 240''$. Time goes from left to right and top to bottom.

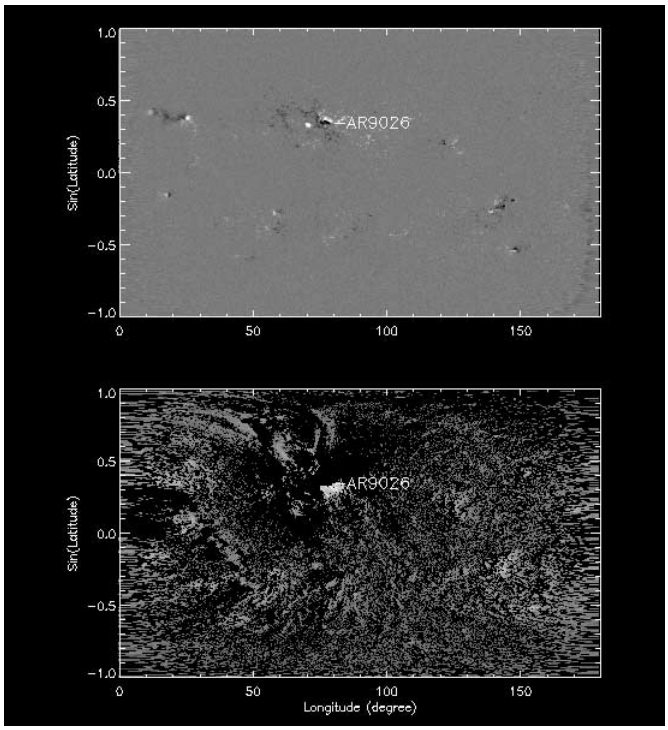

FIG. 22.—Same as Fig. 12, but for the MDI magnetogram taken at 16:00 UT and the EIT images taken at 15:36 UT and 15:48 UT of 2000 June 6.

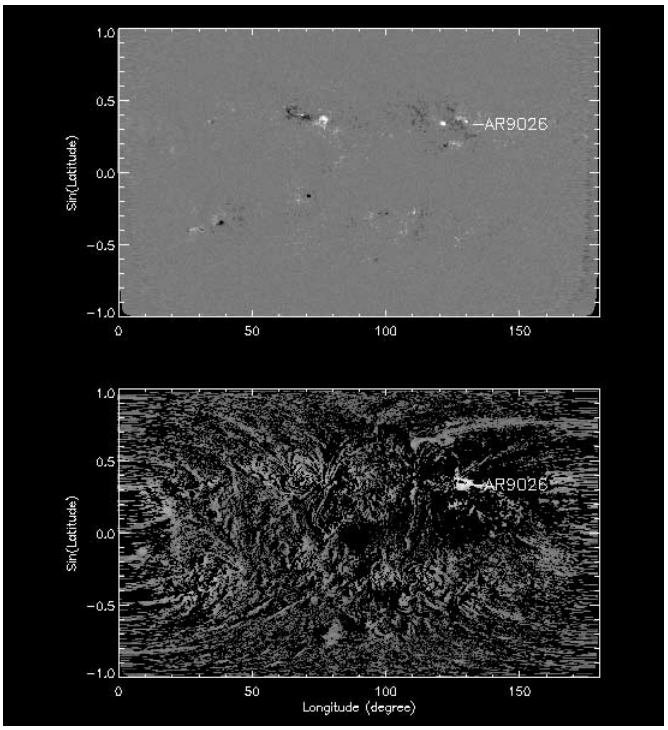

FIG. 24.—Same as Fig. 12, but for the MDI magnetogram taken at 16:00 UT and the EIT images taken at 16:48 UT and 17:24 UT of 2000 June 10.

We noticed that flare F1 was an M-class flare, weaker than the other two (F2 and F3) in the same active region, and that flare F9 is also weaker than F7–8 in AR 9026. Both flares did not cause any geomagnetic storms. However, we feel that importance of the flares in the events analyzed here may not be a key factor in determining whether or not a geomagnetic storm occurs but that the configuration of the erupted magnetic field is. In fact, there has been evidence to support this conjecture. For example, in a statistical research, Cane et al. (2000) demonstrated that "the geoeffectiveness of ejecta depends strongly on the southward magnetic field strength"; Zhang et al. (2003) also concluded, by analyzing 27 major geomagnetic storms in the time period between 1996 and 2000, that no correlation was found between occurrence of major geomagnetic storms and the speed of the associated CMEs, the importance of associated flares, and the association of filament eruptions.

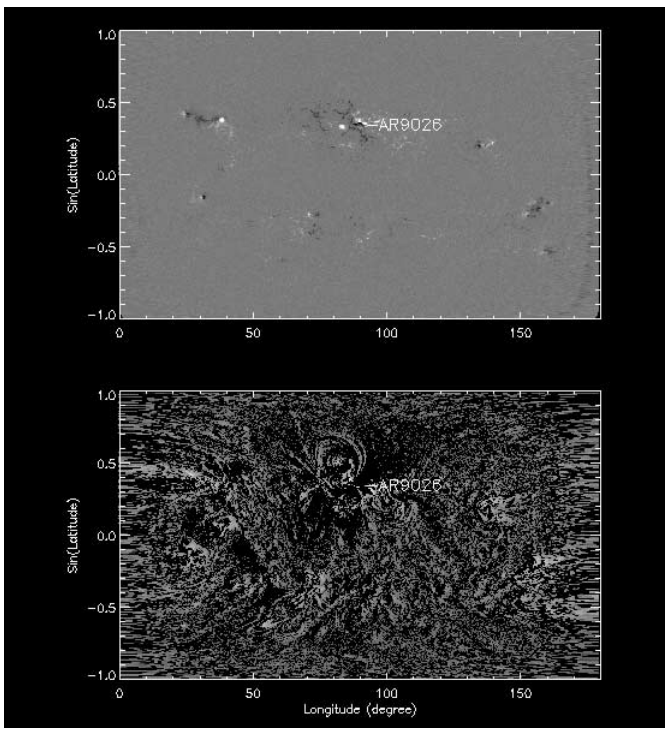

FIG. 23.—Same as Fig. 12, but for the MDI magnetogram taken at 16:00 UT and the EIT images taken at 16:00 UT and 16:24 UT of 2000 June 7.

A possible interpretation of our result involves reformation of the magnetic field configuration after eruption. There have been frequent observations that record such reformations. For example, Hiei et al. (1993) reported reformation of a streamer after an eruption of a prominence, while reformation of filaments has been widely observed for decades (see, e.g., Martin 1973; Tang 1986). The reformed magnetic field, which is identical (or very similar) to the previous magnetic configuration, is likely to yield another similar eruption. Thus, the recurrence of flares and/or CMEs in essentially the same or close locations is a natural consequence of this scenario, and the magnetic configurations involved in the events will be very similar. Such magnetic configurations, when they form the core part of a CME, expand into interplanetary space and can make them very geoeffective. In fact, such a magnetic link was already proposed 20 years ago by Marubashi (1986) to establish a correlation between eruptive filaments and the magnetic clouds. He first demonstrated in two cases the close relationship between the magnetic field configuration of magnetic clouds and the solar magnetic field around the solar filaments and then suggested that "solar magnetic fields overlying a disappearing filament already have a flux rope structure at the time of eruption, and that this structure is extended through interplanetary space to be observed as" a magnetic cloud (Marubashi 1997). As supporting evidence, agreement of the chirality of magnetic clouds and their related filaments was also found by Rust (1994) and Bothmer & Rust (1997).

Our result may, in fact, provide an interpretation for what Leamon et al. (2004) found: compared to the much stronger correlation between magnetic clouds and eruptive filaments (see, e.g., Marubashi, 1986, 1997; Wilson & Hildner 1986; Rust 1994; Bothmer & Schwenn 1994; Bothmer & Rust 1997), there is no systematic sign or amplitude relationship between the magnetic twists of magnetic clouds and their related active regions. We argue that the reason for this discrepancy probably is that the twist of an active region they measured is only an average twist of the whole active region, and not that of the magnetic field actually involved in the eruptive event. This average twist cannot always represent the properties of the erupted magnetic tubes (or flux rope) in the CME. On the other hand, the eruptive filaments themselves are indeed representative of the magnetic field that is actually involved in the eruptions and therefore represent the nature of the magnetic field in the CMEs. Thus, it is not surprising that the relationship between magnetic clouds and their associated eruptive filaments can be well established, but that between active regions and magnetic clouds cannot.

The alignment of the observations from various instruments is a formidable task. We greatly appreciate the mapping software of D. Zarro and the availability of the SSW, which make the alignment much easier. We wish to thank the anonymous referee for the valuable suggestions that have helped improve the manuscript. We thank J. Zhang at Beijing Astronomical Observatory, Kwasan and Hida Observatories, and J. Qiu at BBSO for the Hα data. X. P. Z. and Y. L. were supported at Stanford University by NASA NAG5-13261, the NSF/CISM project under grant ATM 01-20950 and the Department of Defense MURI grants. D. F. W. was supported at Boston College by Air Force contract AF19638-00-K-0073 and NASA grant NAG5-10833. *SOHO* is a project of international cooperation between ESA and NASA.

REFERENCES

Bothmer, V., & Rust, D. M. 1997, in Coronal Mass Ejections, ed. N. Crooker, J. A. Joselyn, & J. Feynman (Geophys. Monogr. 99; Washington: AGU), 139
Bothmer, V., & Schwenn, R. 1994, Space Sci. Rev., 70, 215
Burton, R. K., McPherron, R. L., & Russell, C. T. 1975, J. Geophys. Res., 80, 4204
Cane, H. V., Richardson, I. G., & St. Cyr, O. C. 2000, Geophys. Res. Lett., 27, 3591
Crooker, N. U. 2000, J. Atmos. Sol.-Terr. Phys., 62, 1071
Delannee, C., & Aulanier, G. 1999, Sol. Phys., 190, 107
Hale, G. E., & Nicholson, S. B. 1938, Magnetic Observations of Sunspots 1917–1924 (Publ. Carnegie Inst. 498; Washington: Carnegie Inst.)
Hiei, E., Hundhausen, A. J., & Sime, D. G. 1993, Geophys. Res. Lett., 20, 2785
Leamon, R. J., Canfield, R. C., Jones, S. L, Lambkin, K., Lundberg, B. J., & Pevtsov, A. A. 2004, J. Geophys. Res., 109, A05106
Leamon, R. J., Canfield, R. C., & Pevtsov, A. A. 2002, J. Geophys. Res., 107, 1234, DOI: 10.1029/2001JA000313
Liu, Y., Zhao, X., Hoeksema, J. T., Scherrer, P. H., Wang, J., & Yan, Y. 2002, Sol. Phys., 206, 333
Martin, S. F. 1973, Sol. Phys., 31, 3
Marubashi, K. 1986, Adv. Space Res., 6, 335
———. 1997, in Coronal Mass Ejections, ed. N. Crooker, J. A. Joselyn, & J. Feynman (Geophys. Monogr. 99; Washington: AGU), 147
Pevtsov, A. A., & Canfield, R. C. 2001, J. Geophys. Res., 106, 25191
Richardson, I., et al., 2006, J. Geophys. Res., submitted
Rust, D. M. 1994, Geophys. Res. Lett., 21, 241
Scherrer, P. H., et al. 1995, Sol. Phys., 162, 129
Tang, F. 1986, Sol. Phys., 105, 399
Wang, H., et al. 2000, ApJ, 536, 971
Webb, D. F., Cliver, E. W., Crooker, N. U., St. Cyr, O. C., & Thompson, B. J. 2000, J. Geophys. Res., 105, 7491
Webb, D. F., Crooker, N. U., Plunkett, S. P., & St. Cyr, O. C. 2001, in Space Weather, ed. P. Song, H. Singer, & G. Siscoe (Geophys. Monogr. 125; Washington: AGU), 123
Wilson, R. M., & Hildner, E. 1986, J. Geophys. Res., 91, 5867
Yan, Y., & Sakurai, T. 2000, Sol. Phys., 195, 89
Zhang, J., Dere, K. P., Howard, R. A., & Bothmer, V. 2003, ApJ, 582, 520
Zhang, J., Dere, K. P., Howard, R. A., Kundu, M. R., & White, S. 2001, ApJ, 559, 452
Zhang, J., & Wang, J. 2001, ApJ, 554, 474
Zhao, X. P., & Webb, D. F. 2003, J. Geophys. Res., 108, 1234, DOI: 10.1029/2002JA009606